ChemComm

Selective Hydrosilylation of Olefins by a Two-Dimensional Rh(I) Low-Valent Metal–Organic Framework

Journal:	*ChemComm*
Manuscript ID	CC-COM-04-2025-002201.R2
Article Type:	Communication

ChemComm

COMMUNICATION

Selective Hydrosilylation of Olefins by a Two-Dimensional Rh(I) Low-Valent Metal–Organic Framework

Dipendu Mandal, Madison R. Esposito, Samuel E. Griffin, Grant P. Domecus, and Seth M. Cohen*[a]

pReceived 00th January 20xx,
Accepted 00th January 20xx

DOI: 10.1039/x0xx00000x

Multitopic phosphine ligands combined with Rh(I) or Ir(I) nodes are shown to assemble into low-valent metal-organic frameworks (LVMOFs) with a two-dimensional (2D) topology. The 2D Rh(I) LVMOF exhibits catalytic activity for the hydrosilylation of olefins, functioning in a heterogeneous and selective manner.

Low-valent metal-organic frameworks (LVMOFs) represent an emerging class of materials within the broader field of MOFs.[1] Unlike conventional MOFs, LVMOFs employ secondary building units (SBUs) composed of low-valent metal ions or metal ion clusters coordinated with soft Lewis basic ligands, instead of the high oxidation state metal ions and hard Lewis basic ligands of conventional MOFs.[2] Early examples of LVMOFs were reported by Robson et al. in 1989, featuring coordination networks constructed from tetratopic cyano linkers and CuI nodes.[3, 4] More recent advancements include reports by Figueroa et al. on the use of sterically encumbered isocyanide ligands to construct the LVMOFs $[Cu(CNAr^{Mes2})]_n[PF_6]$ with Cu^I nodes and $[Ni(CNAr^{Mes2})]_n$ (Mes = 2,4,6-Me_3-C_6H_3) with Ni^0 nodes.[5-7] Pederson et al. have employed pyrazine/pyridyl ligands in conjunction with group 6 metal carbonyl complexes $M(CO)_6$ (M=Cr^0, Mo^0, W^0) to prepare LVMOFs $[fac\text{-}M(CO)_3(pyz)_{3/2}]_n$ (pyz = pyrazine; M = Cr^0, Mo^0, W^0), and $[fac\text{-}M(CO)_3(bpy)_{3/2}]_n$ (bpy = bipyridine; M = Mo^0, W^0).[8, 9] Pederson et al. have also recently described the use of preformed, low-valent metal clusters for the preparation of LVMOFs.[10-12] These examples underscore the potential of LVMOFs to facilitate the design of innovative materials with tuneable metal nodes and distinctive reactivity. Additionally, stabilizing low-valent metals in rigid frameworks may reduce deleterious metal leaching, thereby generating more stable, recyclable heterogeneous catalyst systems. Embedding catalytically inefficient homogeneous species into these robust, crystalline heterogeneous platforms may also allow for enhanced activity and stability.

Low-valent metals can form 1D and 3D LVMOFs using tetratopic phosphine ligands (Figure 1).[13] Tetratopic ligands **Si1** and **Sn1** (Fig. 1) produced 3-dimensional (3D), crystalline LVMOFs with Pd^0 and Pt^0 nodes when combined with appropriate metal sources in the presence of a PPh_3 modulator. Similarly, 1-dimensional (1D) LVMOFs (coordination polymers) have been formed with Rh^I and Ir^I using tetratopic phosphine ligands.[13, 14] In these examples, the formation of 1D vs. 3D phases can be explained by the differences in the coordination geometry preferences of the metal centres. Herein, it is shown that a seemingly minor change to the central atom of the tetratopic phosphine ligand can induce the formation of a novel 2D LVMOF phase. Furthermore, the Rh^I derivative is shown to exhibit catalytic activity in the hydrosilylation of olefins.

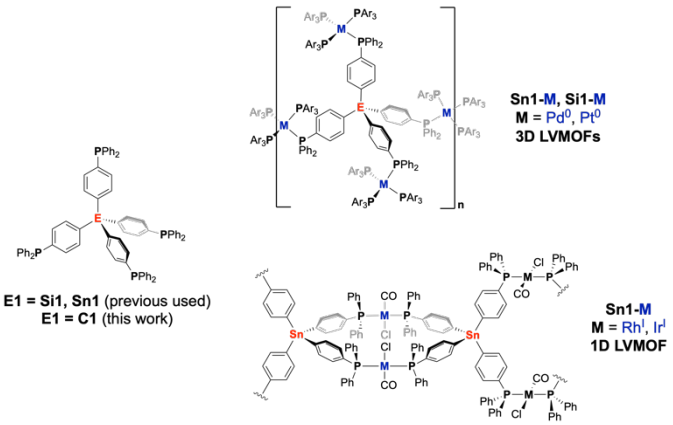

Figure 1. Tetratopic phosphine ligands **C1**, **Si1**, and **Sn1** (E = C, Si, Sn). Tetratopic phosphine ligands **Si1** and **Sn1** have been shown to form 3D LVMOFs with Pd^0 and Pt^0 (*top*), but **Sn1** has been shown to form 1D LVMOFs with Rh^I and Ir^I (*bottom*).

Using the same tetratopic ligand design as **Si1** and **Sn1**, a new ligand with a carbon core (designated **C1**) was synthesized (see ESI for details). It was expected that **C1** would readily generate materials similar to **Si1** and **Sn1**; however, synthesis

Department of Chemistry and Biochemistry, University of California, San Diego, La Jolla, California, 92093, USA. E-mail: scohen@ucsd.edu

Supplementary Information available: Synthesis and characterization details, experimental details for catalysis and recyclability of the catalysts, GCMS chromatograms for optimizations and reactions scope. CCDC XXXXX (C1-Rh) and XXXX (C1-Ir). See DOI: 10.1039/x0xx00000x

conditions similar to those reported for **Sn1-Rh** failed to give any crystalline material.[13] Exploration of alternative reaction conditions revealed that a THF solution containing 2 equiv. of $[RhCl(CO)(PPh_3)_2]$ and **C1** (1 equiv.) at 80 °C for 5-7 d under inert atmosphere (Scheme 1) afforded yellow irregular shape crystals suitable for single crystal X-ray diffraction (SCXRD, Figure 2). $[IrCl(CO)(PPh_3)_2]$ (Vaska's complex) with **C1** similarly yielded yellow crystals suitable for SCXRD (under similar conditions, but at more elevated temperature, 100 °C, see ESI for details). Notably, these initial reaction conditions for producing materials (designated as **C1-Rh** and **C1-Ir**) excluded the use of PPh_3 as a modulator, which was previously found to be essential for the formation of LVMOFs with **Si1** and **Sn1**. However, after these initial conditions were identified, it was determined that incorporation of a modulator could significantly shorten the reaction time; specifically, a mixture of 2.0 equiv. $[RhCl(CO)(PPh_3)_2]$ or $[IrCl(CO)(PPh_3)_2]$, **C1** (0.014 mmol), and P(*o*-Tol)$_3$ (4.0 equiv.) in THF at elevated temperature yielded identical crystalline material in <48 h (see ESI for details).

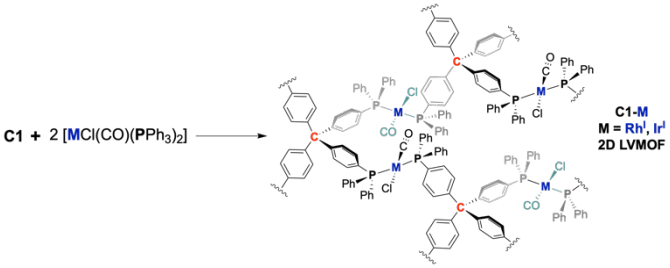

Scheme 1. Synthesis of LVMOFs **C1-Rh** and **C1-Ir**.

Initial SCXRD unit cell parameters of **C1-Rh** and **C1-Ir** showed that these materials were different from the 1D networks of **Sn1-Rh** and **Sn1-Ir**. The structures of **C1-Rh** and **C1-Ir** were orthorhombic in the *Fddd* space group (unlike tetragonal *I4/m* for **Sn1-Rh** and **Sn1-Ir**). In **C1-Rh** and **C1-Ir**, the asymmetric unit {M(CO)Cl(**C1**)$_{1/4}$} (M = Rh, Ir) is assembled into a tetrahedral {(M(CO)Cl)$_4$-**C1**} (M = Rh, Ir) arrangement where four separate metal nodes are connected to two distinct **C1** linkers resulting in an extended 2D network (Figure 2). These constitute a 4,2-connected 2D network (Figure 2). The metal centres retain a square planar geometry, and there are no counter ions in the lattice, indicating the metals remain in the 1+ oxidation state. The metal oxidation state was confirmed by FTIR spectroscopy of **C1-Rh**, which exhibits a ν_{CO} (1971 cm^{-1}) comparable to that of **Sn1-Rh** (1967 cm^{-1}) and the analogous molecular complex $[Rh(CO)Cl(PPh_3)_2]$ (1961 cm^{-1}) (Figure S1), indicating that the electronic environments of these metal centres are the same. Similarly, the FTIR spectrum analysis of **C1-Ir** shows a ν_{CO} of 1968 cm^{-1} akin to that of the molecular $[Ir(CO)Cl(PPh_3)_2]$ (1966 cm^{-1}) complex, corroborating the preservation of the oxidation state at the iridium centre (Figure S2). The differences in framework structures of **C1-Rh/Ir** vs. **Sn1-Rh/Ir** is attributed to the smaller size of the central carbon atom of the tetratopic linker. In **C1-Rh**, the mean bond length between the central carbon (C_{cent}) atom and the aromatic carbon atoms (C_{Ar}) is *ca.* 1.52 Å, with the corresponding C_{Ar}-C_{cent}-C_{Ar} bond angles spanning from *ca.* 103.7-115.2°. **Sn1-Rh** exhibits a notably elongated Sn-C_{Ar} bond distance of 2.14 Å with a geometry around the Sn centre of C_{Ar}-Sn-C_{Ar} bond angles ranging from 107.5-113.4°. In **C1-Ir**, the average bond length between atoms C_{cent} and C_{Ar} is *ca.* 1.66 Å, with the corresponding C_{Ar}-C_{cent}-C_{Ar} bond angles of *ca*. 97.7-127.2°, while **Sn1-Ir** displays an elongated Sn-C_{Ar} bond distance of 2.14 Å and corresponding C_{Ar}-Sn-C_{Ar} bond angles of 108.0-112.4°. These bond metrics underscore the structural differences between the central C and Sn atoms, which manifests as substantial changes in the topology of each material. Hence, the small structural change of the central atom greatly influences the structure of the LVMOF.

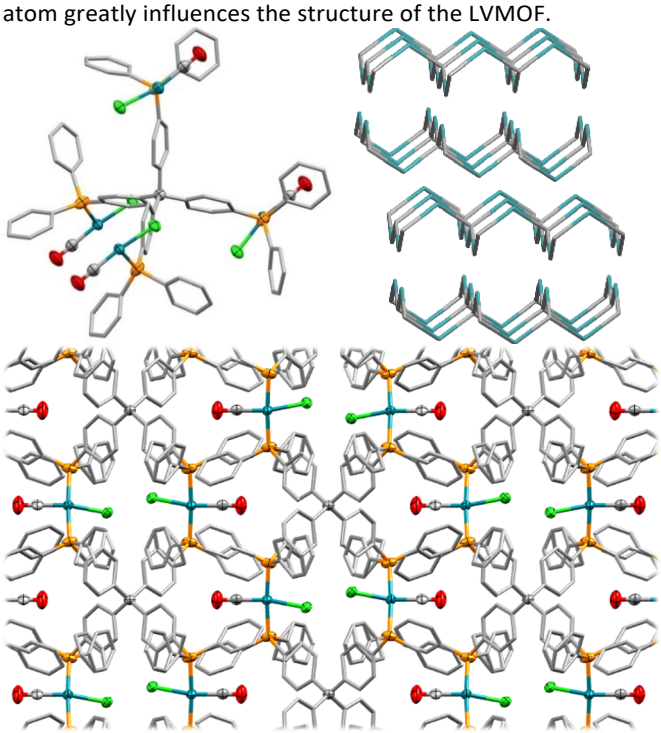

Figure 2. *Top Left*: View of extended repeat unit in **C1-Rh** showing full metal and ligand connectivity. Color scheme: C = gray, Cl = green, O = red, P = orange, Rh = teal; hydrogens omitted for clarity. *Top Right*: Simplified diagram of the 4,2-connected **C1-Rh** 2D network topology. *Bottom*: Packing diagram of **C1-Rh**.

Powder X-ray Diffraction (PXRD) confirmed crystallinity of the bulk materials and showed good agreement with the simulated PXRD pattern of **C1-Rh** and **C1-Ir** (Figure S3). **C1-Rh** retains excellent crystallinity under ambient conditions (>59 d) as confirmed by PXRD and FTIR analysis (Figure S5-S6). The thermal stability of **C1-Rh** was assessed through thermogravimetric analysis (TGA), which indicated a decomposition temperature of ca. ~368 °C. This represents an increase of ~28 °C compared to **Sn1-Rh** and ~134 °C higher than molecular complex $[Rh(CO)Cl(PPh_3)_2]$ (Figure S8). Similarly, TGA analysis of **C1-Ir** displayed a decomposition temperature of ca. ~377 °C, exceeding that of the **Sn1-Ir** material by ~27 °C and surpassing the molecular complex $[Ir(CO)Cl(PPh_3)_2]$ by ~102 °C.[14] Notably, activated samples of **C1-Rh** displayed no uptake of N_2 at cryogenic temperatures (Figure S12).

The application of LVMOFs in heterogeneous olefin hydrosilylation was investigated. Hydrosilylation is a pivotal process for synthesizing organosilicon compounds through the catalytic addition of Si-H bonds to olefins. The resulting products find extensive use in the preparation of silicone-based polymers, rubbers, oils, and various coupling reagents.[15-17] Among the numerous Rh^{I} complexes employed in homogeneous hydrosilylation catalysis, Wilkinson's catalyst $[RhCl(PPh_3)_3]$ has been widely reported to facilitate hydrosilylation reactions.[18, 19]

As a model substrate, 1-octene was combined with triethyl silane (Et_3SiH) as a silylating reagent. Starting with a control reaction of 1-

octene (2.0 equiv.) with Et_3SiH (1.0 equiv.) in 1 mL toluene at 80 ˚C for 24 h without catalyst yielded no hydrosilylation product (Table 1, entry 1). By contrast, the same reaction performed in presence of 0.28 mol% **C1-Rh** in toluene at 25 ˚C for 24 h gave <1% yield of triethyl(octyl)silane hydrosilylation (HS) and <1% of the dehydrogenative silyation (DS) byproduct (Table 1, entry 2). When the reaction temperature was raised to 80 ˚C either in toluene or benzene under otherwise similar conditions, the reaction produced 39±1% (*n*=3) of the HS product and <4±1% (*n*=3) of DS (Table 1, entries 3, 4). During the hydrosilylation process, isomerization of 1-octene to internal octenes was observed. This was confirmed by ^{1}H NMR analysis of the crude reaction mixtures, which showed changes in the position of double bonds within the 1-octene structure (Figure S22). This isomerization typically occurs due to the action of the catalyst under the reaction conditions and is a common side reaction in hydrosilylation.[20] Different solvents were tested including THF and $CDCl_3$ but these yielded HS products in only 22% and 23%, respectively, showing no significant improvement in selectivity compared to toluene (Table 1, entries 5, 6). The employment of **C1-Ir** LVMOF as a heterogeneous catalyst yielded no detectable hydrosilylation product under the same reaction conditions (Table 1, entry 7). Importantly, the analogous molecular complex, $[Rh(CO)Cl(PPh_3)_2]$, showed reduced catalytic activity relative to **C1-Rh**, yielding just 4±2% (*n*=3) HS and 3±1% (*n*=3) DS (Table 1, entry 8). Additionally, Wilkinson's catalyst $[RhCl(PPh_3)_3]$ was tested in the hydrosilylation of 1-octene with Et_3SiH, producing 28±3% (*n*=3) of HS and 2±1% (n=3) of DS products (Table 1, entry 9).

To evaluate a material with identical active sites but a different topology, the previously reported 1D coordination polymer **Sn1-Rh** was evaluated under identical catalytic conditions. Hydrosilylation of 1-octene with **Sn1-Rh** and Et_3SiH in toluene produced 30% HS and 5% DS yield (Table 1, entry 10). The structurally analogous **Sn1-Ir** displayed no catalytic activity in the silylation of 1-octene under identical conditions (Table 1, entry 11).

Table 1. Summary of the optimization of hydrosilylation (HS) product and dehydrogenative silyation (DS) byproduct of 1-octene with $HSiEt_3$.

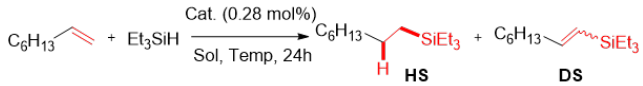

HS DS

Entry	Cat.	Sol.	Temp.	Yield HS (%)[a]	Yield DS (%)[a]
1	-	Toluene	80 °C	0%	0%
2	**C1-Rh**	Toluene	25 °C	<1%	<1%
3[b]	**C1-Rh**	Toluene	80 °C	39±1%	3±1%
4	**C1-Rh**	Benzene	80 °C	40%	3%
5	**C1-Rh**	THF	70 °C	22%	2%
6	**C1-Rh**	$CDCl_3$	70 °C	23%	3%
7	**C1-Ir**	Toluene	80 °C	0%	0%
8[b]	$Rh(CO)Cl(PPh_3)_2$	Toluene	80 °C	4±2%	3±1%
9[b]	$RhCl(PPh_3)_3$	Toluene	80 °C	28±3%	2±1%
10	**Sn1-Rh**	Toluene	80 °C	30%	5%
11	**Sn1-Ir**	Toluene	80 °C	0%	0%
12[c,d]	**C1-Rh**	Toluene	80 °C	>99±0%	0%
13[c]	**Sn1-Rh**	Toluene	80 °C	>99%	0%

[a] Conditions: 0.6 mmol of alkene, 0.3 mmol of silane, toluene (1.0 mL), 80 °C, 24 h (see ESI for details). Yields determined by GCMS with *n*-dodecane internal standard. [b] Yields are based on three independent experiments (*n* = 3). [c] Use of $PhMe_2SiH$ instead of Et_3SiH. [d] Yields are based on two independent experiments (*n* = 2).

The use of an alternative silane, dimethylphenylsilane ($PhMe_2SiH$), due to its combination of lower steric hindrance and enhanced reactivity from the phenyl group, resulted in a significant improvement in both yield and selectivity of the hydrosilylation reaction. When the reaction was conducted with either **C1-Rh** or **Sn1-Rh** as the catalyst at 80 °C for 24 h in toluene, the yield of the HS product was >99%, with no DS byproduct detected (Table 1, entries 12 and 13). These findings underscore the importance of both the catalyst and the choice of silane in achieving high efficiency and selectivity in silylation reactions.

To ensure that catalysis was occurring in a heterogenous manner, filtration tests were conducted. Inductively coupled plasma mass spectrometry (ICP-MS) analysis of the filtrate revealed no dissolution of metal species (see ESI for details). Furthermore, the recyclability of the **C1-Rh** catalyst was demonstrated over three reaction cycles (Cycle I: 35±6% HS, 3±1% DS (*n*=2); Cycle II: 37±8% HS, 3±1% DS (*n*=2); Cycle III: 45±5% HS, 4±0% DS (*n*=2)) with 1-octene and Et_3SiH under optimized conditions, without compromising the integrity of the crystalline network and with no dissolution of metal species (Figure S23, see ESI for details). Compared to the molecular $[Rh(CO)Cl(PPh_3)_2]$ complex, **C1-Rh** offers superior stability, ease of recovery, and reusability.

Having established optimized conditions for 1-octene, a focused investigation with a range of other olefins and silanes was subsequently conducted. Employing **C1-Rh** (0.28 mol%) at 80°C for 24 h in toluene, long-chain alkenes showed good selectivity: 1-pentene (31±8% HS; 0% DS), 1-hexene (28±5% HS; 0% DS), 1-heptene (37±3% HS; 2±1% DS), and 4-phenyl-1-butene (85±9% HS; 0% DS) yielded exclusively silylation products (based on three independent experiments, *n*=3, Figure 3). By contrast, allyl-pentafluorobenzene gave 11±2% of HS and 9±1% DS (*n*=2) byproduct. Styrene derivatives, including 4-chlorostyrene, demonstrated significantly lower yields, producing 9±1% HS and 29±2% DS (*n*=2). This suggests that the electronic nature of the substrate plays a crucial role in influencing the selectivity and efficiency of hydrosilylation reactions. In contrast, 2-methyl-1-heptene yielded 2±1% HS (*n*=3) product, indicating that the increasing steric hindrance of the olefin markedly impedes the reaction kinetics. When the silane source was changed to $PhMe_2SiH$, a large enhancement of yield was observed for 1-hexene (>99% HS; 0% DS), 1-heptene (>99% HS; 0% DS), 1-octene (>99±0% HS; 0% DS) and 4-phenyl-1-butene (>99% HS; 0% DS) with the exclusive formation of HS products (Figure 3). Furthermore, the natural product methyl eugenol was successfully silylated with excellent selectivity and yield utilizing either **C1-Rh** (>99% HS; 0%DS) or **Sn1-Rh** (>99% HS; 0%DS) as the catalyst. Conversely, silyation of 1-octene with the use of sterically hindered and electron deficient triethoxysilane ($(EtO)_3SiH$), yielded no detectable HS products. These findings underscore the importance of both silane reactivity and substrate electronic characteristics in determining the outcomes of these hydrosilylation reactions.

In conclusion, this study has elucidated that the topology of LVMOFs exhibits a remarkable sensitivity to even subtle modifications of tetratopic phosphine ligands. While the tetratopic linkers **C1** and **Sn1** are topologically similar, the stereo-electronic influence of employing carbon as a core atom induced the formation of a 2D framework for **C1-Rh**, which is distinct from the 1D coordination polymer of **Sn1-Rh**. **C1-Rh**, **C1-Ir**, **Sn1-Rh**, and **Sn1-Ir** were investigated for their catalytic activity in silylation reactions. **C1-Rh** and **Sn1-Rh** were found to catalyze the silylation of olefins with varying selectivity and

efficiency depending on the substrates. This study highlights the new structures and new catalysts that can be discovered within the realm of LVMOFs.

The data supporting this article have been included as part of the Supplementary Information. Crystallographic data for **C1-Rh** and **C1-Ir** has been deposited at the CCDC under deposition numbers 2419327-2419328 and can be obtained from https://www.ccdc.cam.ac.uk.

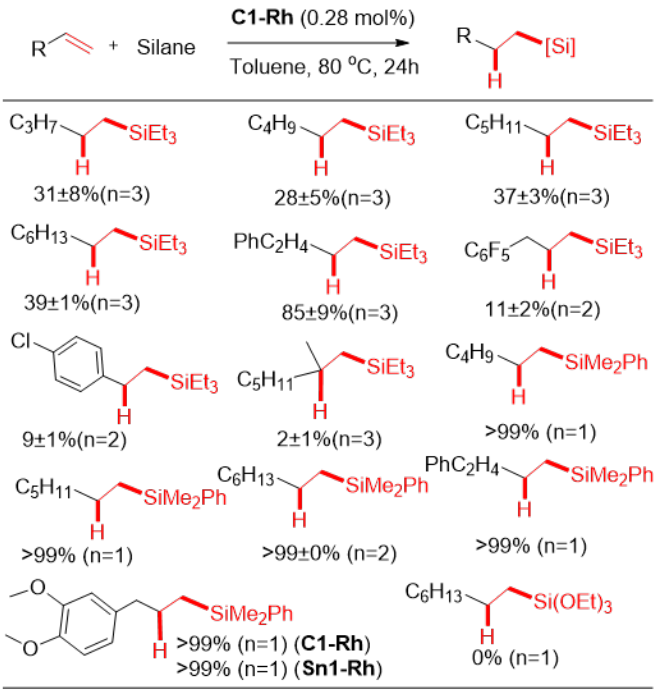

Figure 3. Reaction scope of olefins and silanes for HS reaction. Reaction conditions: 0.6 mmol of alkene, 0.3 mmol of silane, toluene (1.0 mL), 80 °C, 24 h (see ESI for details). Yields were determined by GCMS using an internal *n*-dodecane standard.

This research was supported by the National Science Foundation (Award No CHE-2153240). M.R.E was supported in part by a San Diego Fellowship awarded by the UC San Diego Materials Research Science and Engineering Center (UCSD MRSEC, DMR-2011924). We thank Prof. Joshua Figueroa (UCSD) who provided generous access to an inert atmosphere glove box to support these studies. We thank Dr. Jake Bailey (UCSD) for assistance with X-ray crystallography and Dr. Yongxuan Su (Molecular Mass Spectrometry Facility, UCSD) for assistance with GCMS analysis.

Data Availability Statement. The data supporting this article have been included as part of the Supplementary Information.

Conflicts of interest

There are no conflicts to declare.

Notes and references

1. R. E. Sikma, K. P. Balto, J. S. Figueroa and S. M. Cohen, *Angew. Chem. Int. Ed.*, 2022, **61**, e202206353.
2. N. L. Rosi, J. Eckert, M. Eddaoudi, D. T. Vodak, J. Kim, M. O'Keeffe, O. M. Yaghi, *Science*, 2003, **300**, 1127-1129.
3. B. F. Hoskins, R. Robson, *J. Am. Chem. Soc.*, 1989, **111**, 5962–5964.
4. R. Robson, *Chem Rec*, 2024, **24**, e202400038.
5. D. W. Agnew, M. Gembicky, C. E. Moore, A. L. Rheingold and J. S. Figueroa, *J. Am. Chem. Soc.*, 2016, **138**, 15138-15141.
6. D. W. Agnew, I. M. DiMucci, A. Arroyave, M. Gembicky, C. E. Moore, S. N. MacMillan, A. L. Rheingold, K. M. Lancaster and J. S. Figueroa, *J. Am. Chem. Soc.*, 2017, **139**, 17257-17260.
7. A. Arroyave, M. Gembicky, A. L. Rheingold and J. S. Figueroa, *Inorg Chem*, 2020, **59**, 11868-11878.
8. L. Voigt, R. W. Larsen, M. Kubus and K. S. Pedersen, *Chem. Commun.*, 2021, **57**, 3861-3864.
9. C. E. Andersen, J. N. McPherson, M. G.-Marqués, J. Li, M. Kubus, S. Ito, C. R. Göb, S. Ott, R. W. Larsen, G. Minguez Espallargas and K. S. Pedersen, *J. Mater. Chem. C*, 2023, **11**, 11460-11465.
10. J. H. Gillen, C. A. Moore, M. Vuong, J. Shajahan, M. R. Anstey, J. R. Alston and C. M. Bejger, *Chem. Commun.*, 2022, **58**, 4885-4888.
11. K. Kadota, T. Chen, E. L. Gormley, C. H. Hendon, M. Dincă and C. K. Brozek, *Chem. Sci.*, 2023, **14**, 11410-11416.
12. X. Liu, J. N. McPherson, C. E. Andersen, M. S. B. Jorgensen, R. W. Larsen, N. J. Yutronkie, F. Wilhelm, A. Rogalev, M. Gimenez-Marques, G. Minguez Espallargas, C. R. Gob and K. S. Pedersen, *Nat. Commun.*, 2024, **15**, 1177.
13. R. E. Sikma and S. M. Cohen, *Angew. Chem. Int. Ed.*, 2022, **61**, e202115454.
14. S. E. Griffin, G. P. Domecus, C. E. Flores, R. E. Sikma, L. Benz and S. M. Cohen, *Angew. Chem. Int. Ed.*, 2023, **62**, e202301611.
15. B. Marciniec, *Hydrosilylation: A Comprehensive Review on Recent Advances*, 2009, Springer.
16. L. N. Lewis, J. Stein, Y. Gao, R. E. Colborn, G. Hutchins, *Platinum Metals Rev.*, 1997, **41**, 66.
17. T. Komiyama, Y. Minami and T. Hiyama, *ACS Catal*, 2016, **7**, 631.
18. B. Marciniec, *Silicon Chem.*, 2002, **1**, 155.
19. J. B. Baruah, K. Osakada, T. Yamamoto, *J. Mol. Catal.*, 1995, **101**, 17-24.
20. B. B. Sarma, J. Kim, J. Amsler, G. Agostini, C. Weidenthaler, N. Pfander, R. Arenal, P. Concepcion, P. Plessow, F. Studt and G. Prieto, *Angew. Chem. Int. Ed.*, 2020, **59**, 5806-5815.

Data Availability Statement

The data supporting this article have been included as part of the Supplementary Information.